Deletion of the PsaF Polypeptide Modifies the Environment of the Redox-Active Phylloquinone (A_1). Evidence for Unidirectionality of Electron Transfer in Photosystem I

Fan Yang,[†] Gaozhong Shen,[‡] Wendy M. Schluchter,[‡] Boris L. Zybailov,[‡] Alexander O. Ganago,[‡] Ilya R. Vassiliev,[‡,§] Donald A. Bryant,[‡] and John H. Golbeck*[,‡]

Department of Chemistry, University of Nebraska, Lincoln, Nebraska 68588, and Department of Biochemistry and Molecular Biology, The Pennsylvania State University, University Park, Pennsylvania 16802

Received: April 22, 1998; In Final Form: June 26, 1998

The issue of whether one or both branches of electron-transfer cofactors is active in Photosystem I (PS I) was studied using a strategy employing interposon mutagenesis and electron paramagnetic resonance (EPR) spectroscopy. PS I complexes were isolated using *n*-dodecyl-*β*-D-maltoside (DM) or Triton X-100 (TX-100) from wild-type and mutant strains of *Synechococcus* sp. PCC 7002 lacking specific PS I polypeptides. The principal values of the *g*-tensor of A_1 were determined by Q-band (34.0 GHz) EPR spectroscopy of perdeuterated, wild-type PS I complexes as $g_{xx} = 2.0062$, $g_{yy} = 2.0050$, and $g_{zz} = 2.0021$, and a stoichiometry of ≤ 1.0 A_1^- per $P700^+$ was measured by spin quantitation of photoaccumulated, wild-type PS I complexes at illumination temperatures between 195 and 220 K. The characteristic anisotropic EPR spectrum of A_1^- was photoaccumulated in all mutant PS I complexes isolated with DM and most mutant PS I complexes isolated with TX-100; however, A_0^- was photoaccumulated in PS I complexes isolated with TX-100 from the *psaF* and *psaE psaF* mutants. PS I complexes isolated with TX-100 from the wild type and the *psaE psaF* mutant retained 2.5 phylloquinone (PhQ) and 2.6 PhQ per 100 Chl, respectively, indicating that the failure to observe A_1^- in the *psaE psaF* mutant is not due to the loss of PhQ. Steady-state rates of light-induced flavodoxin reduction for PS I complexes isolated with DM and TX-100 from the *psaF* and *psaE psaF* mutants were nearly identical and differed by less than a factor of 2 from that for the wild-type. The inability to photoaccumulate a second A_1^- in the wild-type and the *psaE psaF* mutant indicates that only one of the two resident PhQs in PS I is redox active. The presence of A_0^- in the *psaE* and *psaE psaF* mutants is explained by the protonation and secondary reduction of the semiquinone anion radical of PhQ which is made solvent-accessible by removal of the PsaF polypeptide and by exposure to TX-100. Since only the loss of the C_3-distal PsaF or PsaE and PsaF polypeptides affects the spectroscopic properties of A_1, the binding site of the redox-active PhQ is associated with the nonprimed α-helices assigned to PsaA/PsaB the electron density map.

Introduction

The photosystem I (PS I) reaction center is an iron−sulfur type photooxidoreductase that catalyzes the oxidation of plastocyanin (or cytochrome c_6) in the thylakoid lumen and the reduction of soluble [2Fe−2S] ferredoxin (or flavodoxin) in the stroma. PS I trimers from the thermophilic cyanobacterium *Synechococcus* sp. have been crystallized,[64] and X-ray diffraction analyses have resulted in an electron density map at a resolution of ca. 4 Å.[27] This map has been interpreted to show the primary components of the electron-transfer chain arranged along a pseudo-C_2 (AB) symmetry axis of the PS I monomers and separated from the antenna chlorophylls by a palisade of 10 α-helices (Figure 1A, B).[48] The first pair of Chl *a* molecules, eC_1 and eC_1', of the electron-transfer chains form the symmetric P700 dimer which is oriented parallel to the pseudo-C_2 (AB) axis. Two additional pseudo-symmetric pairs of chlorophylls, eC_2/eC_2' and eC_3/eC_3', form a bifurcating chain of cofactors. One of the latter pair of chlorophylls is presumed to represent the primary acceptor, A_0, while the former pair of chlorophylls are presumed to be analogous to the bridging chlorophylls found in the reaction center of purple bacteria.[14,16] The bifurcating cofactor chain in PS I converges at the interpolypeptide F_X iron−sulfur cluster, after which electron transfer is presumed to occur unidirectionally through F_A and F_B to ferredoxin (reviewed in Brettel[8]).

Two phylloquinones, one of which is known spectroscopically as the secondary electron acceptor A_1, are also present in PS I (reviewed in Golbeck and Bryant[17]). However, the headgroup of the naphthoquinone molecule is similar in size to the side chains of aromatic amino acids, and the phylloquinones have not yet been unambiguously located on the electron density map. Photovoltage measurements show that the transmembrane distance from A_0 to A_1 spans only 20 ± 8% of the P700 to A_1 distance.[23] Because the distance between P700 and A_0 is 22 Å (according to the electron density map[48]), A_1 should be located ca. 26 Å from P700, provided the dielectric is uniform throughout the protein. Pulsed EPR studies of single crystals localize the spin density on A_1^- at a distance 25.4 Å from the radical pair[66] and at an angle of 27 ± 0.5° normal to the membrane.[4] This distance and angle defines a circle which

[†] Department of Chemistry.
[‡] Department of Biochemistry and Molecular Biology.
[§] On leave from the Department of Biophysics, Faculty of Biology, M. V. Lomonosov Moscow State University, Moscow 119899, Russia.
* To whom correspondence should be addressed: Tel, 814 865 1163; Fax, 814 863 7024; e-mail, JHG5@psu.edu.

S1089-5647(98)01952-X CCC: $15.00
Published on Web 08/25/1998

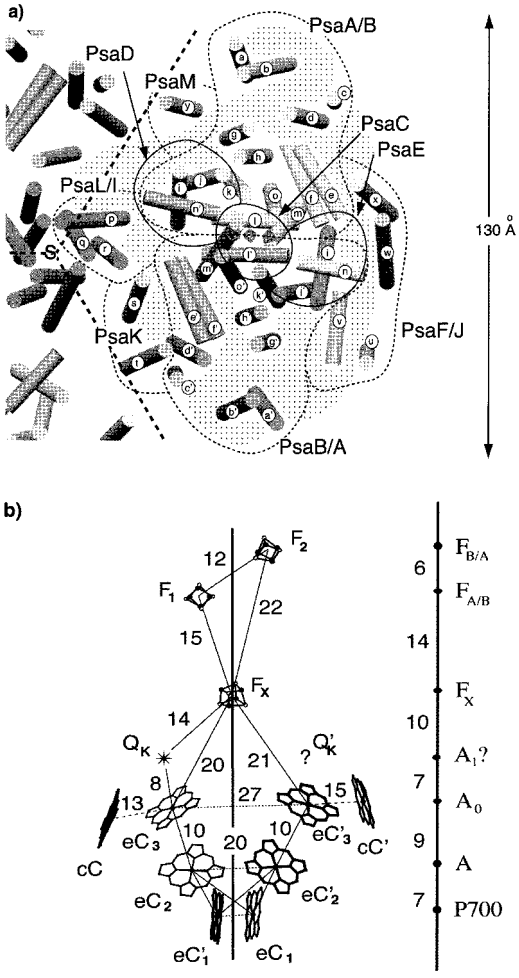

Figure 1. (A) Schematic representation of the transmembrane α-helices of one PS I monomer. Group I polypeptides are composed of the RCs with the deleted subunits on the side of the monomers where the *m*′ and *n*′ α-helices intersect, that is, proximal to the C_3 axis of symmetry represented by the triangle: PsaI, PsaK, PsaL, or PsaM polypeptides. Group II includes the PS I complexes that are missing subunits on the side of the monomers where the *m* and *n* α-helices intersect, that is, distal to the C_3 axis of symmetry represented by the triangle: PsaE, PsaF, or PsaJ polypeptides. (B) Schematic rendering of the cofactors of the electron-transfer system. The proposed location of one of the two phylloquinone molecules is depicted by the symbol (*) and denoted as Q_K. The second phylloquinone is denoted as Q_K' and its location is not assigned. Figures used with permission of Schubert, W. D.; Klukas, O.; Krauss, N.; Saenger, W.; Fromme, P.; Witt, H. T. See Schubert et al. *J. Mol. Biol.* **1997**, *272*, 741−769 for a comprehensive description of the figures.

intersects regions of electron density at two possible locations (Figure 1) which are near the intersection of the *n* (and *n*′) and *m* (and *m*′) helices of PsaA/PsaB (the relationship between the primed and nonprimed helices, as well as that between the PsaA and PsaB polypeptides, is not yet established by X-ray crystallographic analysis).

The existence of this bifurcating chain raises an important question which cannot be addressed by X-ray crystallography: does electron transfer occur through only one branch of the pseudo-symmetric pairs of chlorophylls, as occurs in the bacterial reaction center, or can electron transfer occur through both branches, meeting at the intersection point of F_X? Moreover, if electron transfer only occurs through one of the two branches, which branch is the active branch? We have sought to answer these questions through a combination of interposon mutagenesis and EPR spectroscopic characterization of the photoactive PhQ. Our approach focuses on the nonsymmetry related, transmembrane polypeptides of low molecular mass on each side of either PsaA or PsaB. We reasoned that selective removal of one or more of these polypeptides by mutation could alter the properties of A_1 and shed insight into the pathway of electron transport within PS I. As shown by the data presented here, the removal of some polypeptides selectively modifies the photoaccumulation behavior of the A_1 phylloquinone. These observations allow one to deduce the cofactor branch which is active in electron transport. A preliminary report concerning these studies was presented at the 9th International Congress on Phototrophs in Vienna, Austria in September, 1997.[65]

Materials and Methods

The cyanobacterium *Synechococcus* sp. PCC 7002 was grown in liquid medium A[53] supplemented with 1 mg mL^{-1} $NaNO_3$ (A^+ medium) at 37 °C. Cultures were continuously aerated with 1% (v/v) CO_2. Both wild-type and mutant strains were grown with continuous illumination provided by cool-white fluorescent lamps at an intensity of 250−350 μE m^{-2} s^{-1}. Wild-type cells were also grown in A^+ medium prepared with 99% D_2O at 50 μE m^{-2} s^{-1} at 37 °C. The mutant strains were grown in A^+ medium with the addition of the appropriate antibiotic(s). The *Synechococcus* sp. PCC 7002 mutant strains used in this study were Δ*psaE* (deletion of the *psaE* gene; G. Shen, unpublished results); *psaF* (interruption of the *psaF* gene (Schluchter, W.; Shen, G.; Bryant, D. manuscript in preparation); *psaE psaF* (interruption of the *psaF* gene and deletion of the *psaE* gene Shen, G., unpublished results); *psaI, psaJ, psaK, psaL* (the interruption of appropriate genes[46]); *psaM, psaI psaL, psaK psaL, psaL psaM*, and *psaI psaJ psaL* (interruption of the appropriate genes, Shen, G., unpublished results).

Thylakoid membranes from wild-type and mutant strains of *Synechococcus* sp. PCC 7002 were solubilized in either 30 mM *n*-dodecyl-*β*-D-maltoside or 1% (w/v) Triton X-100. PS I complexes were isolated using two successive sucrose gradients as described.[41] Chlorophyll concentration was determined by extraction with 100% methanol and by measuring the optical density at 663 nm.[28,30] The protein compositions of wild-type and mutant PS I complexes isolated from *Synechococcus* sp. PCC 7002 were determined by SDS polyacrylamide gel electrophoresis as described.[45,47] The polypeptides were visualized by silver staining.[5] Immunoblotting of PS I polypeptides resolved by SDS polyacrylamide gel electrophoresis was performed as previously described.[47,51]

The PhQ content of the wild-type and mutant PS I complexes was determined by chemical extraction and chromatographic analysis. PS I complexes (500 μg Chl mL^{-1}) were exchanged into distilled water by ultrafiltration over a YM-100 membrane and lyophilized for 30 h. The pigments were extracted with 1:1 (v:v) acetone/methanol at 4 °C. The solution was centrifuged and the chlorophyll concentration of the supernatant was determined. A 100 μL aliquot of the extraction mixture was analyzed by reverse phase chromatography over a C_{18} column attached to a Model 2350 high-performance liquid chromatography system (ISCO, Inc., Lincoln, NE). The elutants were monitored using a Model 481 LC spectrophotometer (Millipore, Inc.). The separation was performed using a step gradient of 96% methanol and 4% H_2O for 15 min and 100% methanol for an additional 45 min. The peak with a retention time of 28 min was identified as PhQ by comparison with a standard (Sigma Chemical Co., St. Louis, MO). The PhQ concentration was determined by integrating the peak and comparing it with

a known concentration of authentic PhQ. The molar concentration of the authentic PhQ was determined spectrophotometrically by its absorbance in the near-UV using an extinction coefficient of 16.8 mM^{-1} cm^{-1} at 270 nm.[13]

X-band (9.4 GHz) EPR studies were performed using a Bruker ESP300E spectrometer and an ER/4102 ST resonator. Cryogenic temperatures were maintained with an Oxford Instruments ESR900 liquid helium cryostat and an ITC4 temperature control unit. The microwave frequency was measured with a Hewlett-Packard 5352B frequency counter, and the magnetic field was measured with a Bruker ER035M NMR Gaussmeter. The magnetic field was calibrated with α,α′-diphenyl-β-picryl hydrazyl (DPPH). Q-band (34 GHz) EPR studies were performed using an ER 5106 QT-W1 resonator equipped with a port for sample illumination. Cryogenic temperatures were maintained with an ER4118CV liquid nitrogen cryostat and an ER4121 temperature control unit. The magnetic field was calibrated with γ,γ-bisdiphenylene-β-phenylallyl (BDPA) complexed 1:1 with benzene which has no detectable *g*-anisotopy at 34 GHz.

Photoaccumulation protocols on wild-type and mutant PS I complexes were carried out in a manner similar to that described.[22] Prior to illumination, the pH of the sample was adjusted to 10.0 and sodium hydrosulfite was added to a final concentration of 100 mM. The sample was incubated in darkness for 30 min, placed in a dewar containing a dry ice−ethanol mixture at a temperature of 205 K, and illuminated by passing the output of a focused 100 W quartz−tungsten lamp through a 2.5 cm water filter. The photoaccumulation time was 40 min unless otherwise indicated in the text. After illumination, the sample was immediately frozen in liquid nitrogen, transferred to the cryostat, and the spectrum was acquired at 100 K without additional illumination. The A_0^- radical was photoaccumulated with the same protocol using a P700-A_0 core complex from which the electron-transfer cofactors A_1, F_X, F_A, and F_B had been removed.[62,63]

Spin quantitations were carried out on A_1^- and $P700^+$ by photoaccumulating the radicals directly in the EPR cavity. The A_1^- radical was generated by illuminating PS I complexes with a 20 mW HeNe laser at 205 K in the presence of 25 mM sodium hydrosulfite and 1 M glycine. The $P700^+$ radical was generated by illuminating PS I complexes with a 20 mW HeNe laser as the temperature was lowered to 100 K in the presence of 10 mM sodium ascorbate and 4 μM DCPIP. A matrix of temperature and microwave power levels was initially performed on the sample and the spin standard to ensure that the signal intensities were determined in the Curie law region under nonsaturating conditions, i.e., that the doubly integrated signal intensity is proportional to the square root of the microwave power. A ratio of spins per P700 (per reaction center) was obtained. EPR spectral simulations of A_1^-, A_0^- and $P700^+$ were carried out on a Power Macintosh 8500/250 computer using a Windows 3.1 emulator (SoftWindows 3.0, Insignia Solutions, UK) and SimFonia software (Bruker Analytik GMBH). The relative spin concentrations of A_1^- and A_0^- were determined by visual matching of the experimental photoaccumulated spectrum with an arbitrary admixture of simulated spectra of A_1^- plus A_0^-.

Transient absorbance changes of P700 at 832 nm were measured with a laboratory-built double-beam spectrophotometer described previously.[60] The isolated PS I complexes were resuspended under anaerobic conditions to a chlorophyll concentration of 50 μg mL^{-1} in the presence of 0.05% of Triton X-100 or 0.05% DM (depending on the nature of the detergent used for isolation). To modulate the oxidation state of the terminal iron−sulfur clusters, F_A and F_B, prior to the flash, 25 mM Tris buffer (pH 8.3) with 10 mM sodium ascorbate and 4 μM 2.6-DCPIP (both clusters oxidized) or 100 mM glycine buffer (pH 10) with 100 mM sodium hydrosulfite (both clusters reduced) was used. The excitation was provided by a frequency-doubled, Q-switched Nd:YAG laser (wavelength, 532 nm; flash energy, 5 mJ; fwhm, 15 ns).

Rates of flavodoxin photoreduction were measured in a 1.3 mL volume using wild-type and mutant PS I complexes at 5 μg of Chl mL^{-1} in 50 mM Tricine, pH 8.0, 50 mM $MgCl_2$, 15 μM cytochrome c_6, 15 μM flavodoxin, 6 mM sodium ascorbate, and 0.05% *n*-dodecyl-β-D-maltoside. Measurements were made by monitoring the rate of change in the absorption at 467 nm using a Cary 219 spectrophotometer fitted with an interference filter on the surface of the photomultiplier. The 4-sided (clear) cuvette was illuminated from the both sides using high intensity, red light-emitting diodes (LS1, Hansatech Ltd., Norfolk, UK). The light intensity was saturating at the chlorophyll concentration used in this study.

Results

Polypeptide Composition of PS I Mutants. PS I complexes were prepared using the detergents Triton X-100 (TX-100) or *n*-dodecyl-β-D-maltoside (DM) from membranes of the wild-type strain of *Synechococcus* sp. PCC 7002 and from mutant strains in which the following genes had been deleted or insertionally inactivated: *psaE*, *psaF*, *psaI*, *psaJ*, *psaK*, *psaL*, and *psaM*. Double and triple mutants were also studied in which the following combinations of genes had been deleted or insertionally inactivated: *psaE psaF*, *psaI psaL*, *psaI psaJ psaL*, *psaK psaL*, and *psaL psaM*. The presence or absence of PsaC, PsaD, PsaE, PsaF, and PsaL was verified by a combination of both SDS−PAGE and immunoblotting analyses, while the presence or absence of PsaK and PsaM was verified by SDS−PAGE alone since these proteins were clearly separated on SDS−PAGE. Strains lacking PsaI were created by deletion of the entire coding sequence for the gene[47] and were verified by polymerase chain reaction analyses of the *psaI* locus. Although PsaI and PsaJ of *Synechococcus* sp. PCC 7002 often comigrate on SDS−PAGE,[47] these two polypeptides are differently colored when stained with silver; thus, the presence or absence of PsaJ could be verified by a combination of polymerase chain reaction analyses to verify the gene locus and by comparing mutant and wild-type polypeptide patterns after silver staining. Using DM, PS I complexes isolated from the mutant strains *psaE*, *psaJ*, *psaK*, *psaL*, *psaM*, and various combination mutants were only depleted of the targeted polypeptide(s) (data not shown, but see Figure 2). Because *psaJ* is located immediately downstream from *psaF* and is co-transcribed in *Synechococcus* sp. PCC 7002, and because PsaF and PsaJ are believed to interact strongly in PS I (see Figure 1A), PsaJ was also found to be missing from the PS I complexes prepared from the *psaF* and *psaE psaF* mutant strains.

Using TX-100, PS I complexes isolated from the mutant strains *psaE*, *psaI*, *psaJ*, *psaK*, *psaL*, *psaM*, *psaI psaL*, *psaI psaJ psaL*, *psaK psaL*, and *psaL psaM* were also missing only the targeted polypeptides (Figure 2), but those lacking PsaE and PsaF required special precautions. Prolonged exposure of PS I complexes from the wild-type strain to ≥1% (w/v) TX-100 led to the depletion of PsaE and PsaF (see Figure 3, lane 5) as well as PsaJ (see Figure 2, lane 4). Exposure of wild-type PS I complexes to 2% (w/v) TX-100 during solubilization of thylakoids resulted in a loss of about 75% of the PsaE and PsaF

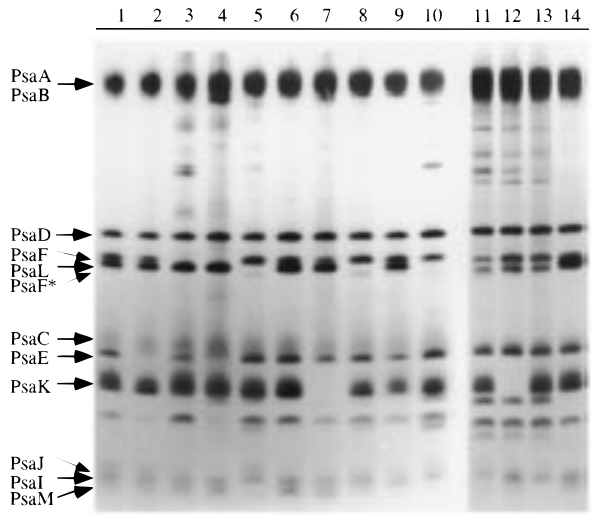

Figure 2. SDS Polyacrylamide gel electrophoresis of PS I complexes isolated from the wild-type and mutant strains of *Synechococcus* sp. PCC 7002. PS I complexes were solubilized from thylakoid membranes (0.4 mg chlorophyll mL^{-1}) using 1% (w/v) TX-100. Proteins corresponding to 2 μg chlorophyll were loaded on each lane of a 16% (w/v) acrylamide gel and visualized by silver staining. Lane 1, wild-type PS I trimers; lane 2, PS I trimers from the *psaE* mutant; lane 3, PS I trimers from the *psaF* mutant; lane 4, PS I trimers from the *psaE psaF* mutant; lane 5, PS I monomers from the *psaI* mutant; lane 6, PS I trimers from the *psaJ* mutant; lane 7, PS I trimers from the *psaK* mutant; lane 8, PS I monomers from the *psaL* mutant; lane 9, PS I trimers from the *psaM* mutant; lane 10, PS I monomers from the *psaI psaJ psaL* triple mutant; lane 11, PS I monomers from the *psaI psaL* mutant; lane 12, PS I monomers from the *psaK psaL* mutant; lane 13, PS I monomers from the *psaL psaM* mutant; lane 14, PS I trimers from the wild-type strain. Monomeric PS I complexes (lanes 5, 8, 10, 11−13) are generally more contaminated with other proteins due to comigration with PS II and other proteins on sucrose density gradients. PS I complexes from *Synechococcus* sp. PCC 7002 consistently contain a polypeptide of ~7 kDa that is not observed in other cyanobacterial PS I complexes; the identity and function of this protein is unknown.

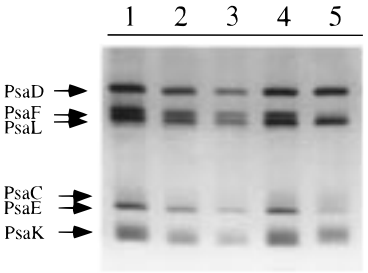

Figure 3. SDS Polyacrylamide gel electrophoresis of PS I complexes isolated from the wild-type strain of *Synechococcus* sp. PCC 7002. The PS I polypeptides were resolved on a 16% (w/v) gel and visualized by silver staining. Lanes 1−3 were contain trimeric PS I complexes prepared with DM and contain the proteins corresponding to 2 μg chlorophyll (lane 1), 1 μg chlorophyll (lane 2), and 0.5 μg chlorophyll (lane 3). Lane 4 shows the protein composition of trimeric PS I complexes (2 μg chlorophyll) prepared by solubilization of thylakoids (0.4 mg chlorophyll mL^{-1}) with 1% (w/v) TX-100 for 1 h. Lane 5 shows damaged trimeric PS I complexes depleted of PsaF and PsaE prepared by solubilization of thylakoids (0.4 mg chlorophyll mL^{-1}) with 2% (w/v) TX-100 for 12 h.

from the complexes (compare Figure 3, lanes 1, 3, and 5). PS I complexes prepared from the *psaF* mutant were also observed to be completely depleted of PsaJ and largely depleted of PsaE under these same conditions (see Mühlenhoff[34]). Similarly, PS I complexes prepared from the *psaE* mutant had decreased amounts of PsaF and PsaJ (data not shown). However, by reducing the solubilization time and the detergent:chlorophyll ratio, it was possible to minimize the loss of these ancillary polypeptides (compare Figure 3, lanes 1, 4, and 5). PS I complexes prepared from the *psaL* mutant were completely lacking PsaI, and nearly 90% of PsaL was missing in the *psaI* mutant even at reduced exposure times and low chlorophyll:detergent ratios (see ref 47). Because the loss of PsaL leads to loss of trimerization,[12,47] monomeric PS I complexes were used in the study of the *psaI* and *psaL* mutants strains.

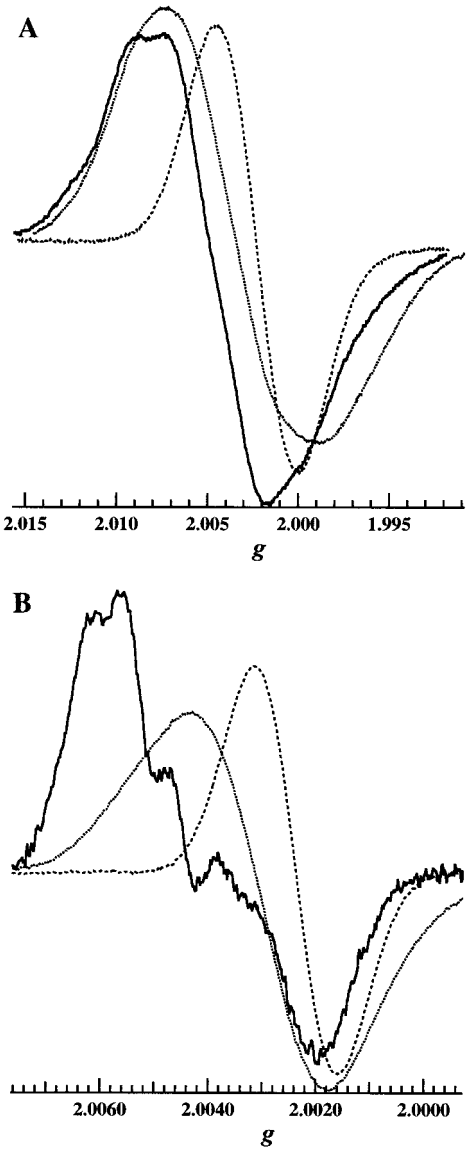

Figure 4. EPR spectra of at 9.4 GHz (A) and 34.0 GHz (B) of A_1^- (solid line) and $P700^+$ (dashed line) in PS I complexes isolated using DM from *Synechococcus* sp. PCC 7002, and A_0^- (dotted line) in P700-A_0 cores isolated using TX-100 from *Synechococcus* sp. PCC 6301. The sample concentration was 1.5 mg chlorophyll mL^{-1}. Conditions for X-band spectra: A_1^-, microwave power, 20 mW; modulation amplitude, 0.2 mT; modulation frequency, 100 kHz; temperature, 100 K. A_0^-: same except microwave power, 63 μW; temperature, 35 K. $P700^+$: microwave power, 63 μW; temperature, 35 K. The A_1^- spectrum was averaged 4 times. Conditions for Q-band spectra: A_1^-, A_0^-, and $P700^+$; microwave power, 53 μW; modulation amplitude, 0.1 mT; modulation frequency, 100 kHz; temperature, 100 K. The A_1^- spectrum was averaged 10 times.

Spectral Resolution of A_0^- and A_1^- at 9.4 and 34.0 GHz. The X-band (9.4 GHz) EPR spectrum of photoaccumulated PS I complexes isolated from the wild-type strain of *Synechococcus* sp. PCC 7002 with DM is depicted in Figure 4A (solid line). The spectrum, with a crossover point at $g = 2.0047$ and the

"peak-to-peak" line width of ca. 10.8 G, is characteristic of the A_1^- radical.[6,33] The EPR spectrum of a photoaccumulated P700-A_0 core is also depicted in Figure 4A (dotted line). This spectrum, with a crossover point at $g = 2.0034$ and a "peak-to-peak" line width of ca. 14 G, is diagnostic of the A_0^- radical.[6,33] The $P700^+$ radical is shown for comparison (Figure 4A, dashed line). It is an unstructured derivative centered at $g = 2.0023$ with a line width of 7.8 G which is narrower than a chlorophyll monomer due to strong electronic coupling between the chlorophyll pairs.[37,43] The overall line shapes of these three organic radicals are governed by two factors: field-dependent *g*-anisotropy and field-independent nuclear−electron hyperfine interactions. At 9.4 GHz, the A_1^- spectrum is dominated by hyperfine interactions, the most prominent of which are electron−nuclear couplings with the three protons on the 2-methyl group.[2,44,57] The A_0^- and $P700^+$ spectra are completely dominated by a large number of unresolved hyperfine couplings and thus appear structureless. Given that the anisotropy of A_1 is not resolved at X-band, the overlap between A_0^- and A_1^- makes it difficult to determine the relative amounts of the two radicals in a given sample.

The Q-band (34.0 GHz) EPR spectrum of photoaccumulated PS I complexes isolated from the wild-type strain of *Synechococcus* sp. PCC 7002 with DM is depicted in Figure 4B (solid line). At this microwave frequency, the field-dependent *g*-anisotropy dominates the spectrum of A_1^-,[56] allowing the principal values of A_1^- to partially resolved, with apparent $g_{xx} = 2.0062$ and g_{zz} of 2.0021. The g_{yy} component of the tensor is obscured by the resolved hyperfine interactions derived from the 2-methyl group. In contrast, the A_0^- radical remains an unstructured derivative centered at $g = 2.0034$ with a line width of 15 G (Figure 4B, dotted line; the asymmetry in the low-field region is probably due to residual A_1^-), and the $P700^+$ radical remains an unstructured derivative centered at $g = 2.0023$ with a line width of 9.2 G (Figure 4B, dashed line). Because the g_{xx} component of A_1^- is separated from the A_0^- resonance, the identity of an unknown radical can be determined solely based on its *g*-anisotropy at Q-band. With the additional knowledge of the principal values of the *g*-tensors of A_1^- and A_0^-, the relative spin concentrations of each radical can be determined by spectral simulations.

The *g*-Tensor and Spin Concentration of A_1^-. To extract the principal values of the *g*-tensor of A_1^-, PS I complexes were isolated from *Synechococcus* sp. PCC 7002 grown in 99% D_2O. As shown in Figure 5A (solid line), the suppression of the hyperfine couplings results in a narrowing of the line width of the A_1 spectrum at Q-band (compare solid lines, Figures 5A, 5B), with the consequence that the g_{yy} component of the spectrum is now resolved from the g_{xx} component. The A_1^- spectrum is simulated using a *g*-tensor with principal values $g_{xx} = 2.0062$, $g_{yy} = 2.0050$, and $g_{zz} = 2.0021$ and line widths of 2.4, 3.7, and 2.4 G, respectively (Figure 5A, dotted line). The major deviations from the simulated spectrum appear principally in the high-field component and include a small contribution from A_0^-. Our extracted *g*-tensor is nearly identical to the principal values of $g_{xx} = 2.0062$, $g_{yy} = 2.0051$, and $g_{zz} = 2.0022$ determined at 95 GHz (W-band) in an electron spin-polarized EPR study of A_1^- in nondeuterated PS I complexes from *Synechococcus lividus*[57] and to the principal values of $g_{xx} = 2.00625$, $g_{yy} = 2.00503$, and $g_{zz} = 2.00227$ determined at 283 GHz in a CW EPR study of nondeuterated *Synechocystis* sp. PCC 6803 membrane fragments.[31] Although the simulated spectrum does not perfectly match the experimental spectrum in the highfield region of Figure 5A, the amount of contaminating A_0^- at $g = 2.0034$ is judged to be minimal in the perdeuterated PS I complexes.

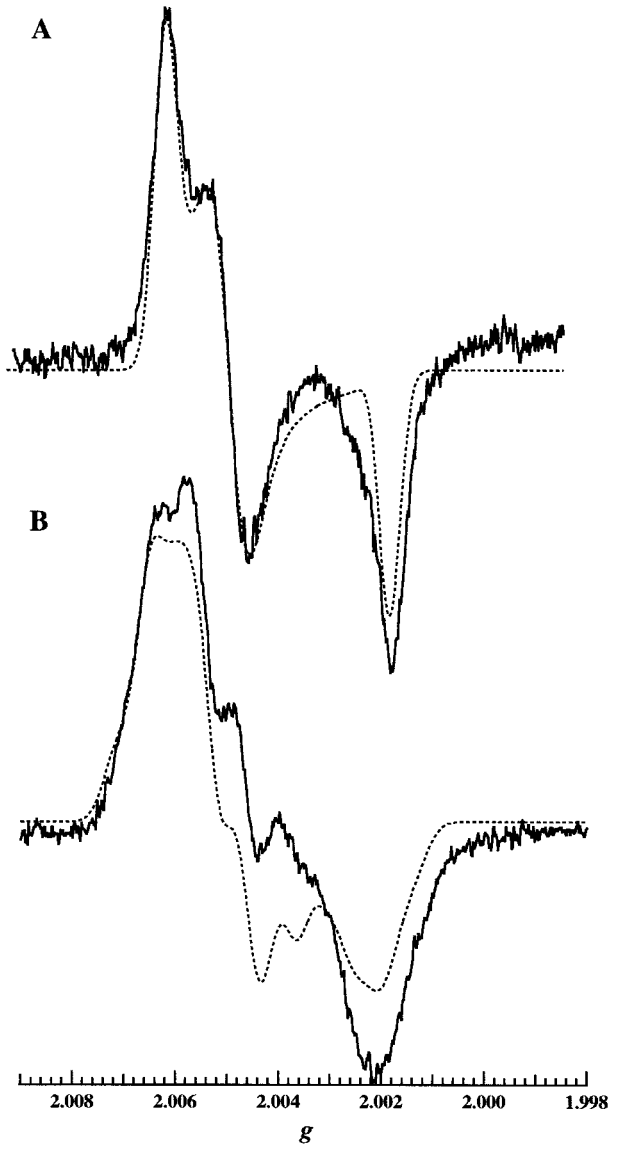

Figure 5. Q-band EPR spectra of wild-type PS I complexes isolated using DM from *Synechococcus* sp. PCC 7002 grown in D_2O (A, solid line) and H_2O (B, solid line). The photoaccumulation was carried out for 40 min at 205 K. The simulated spectrum of A_1^- using $g_{xx} = 2.0062$, $g_{yy} = 2.0050$, and $g_{zz} = 2.0021$ and line widths of 2.4, 3.7, and 2.4 G is shown as the dotted line in A. Instrument conditions: microwave power, 10 μW, modulation amplitude, 0.1 mT, modulation frequency, 100 kHz, temperature, 100 K magnetic field scan, 1.2083 to 1.2203 T; microwave frequency, ca. 34.0874 GHz. The simulated spectrum of A_1^- using the *g*-tensor extracted from the deuterated A_1^- spectrum (A) and an *A*-tensor of 9.0, 12.9, and 9.0 MHz and line widths of 3.25 G for g_{xx}, g_{yy}, and g_{zz} is shown as the dotted line in B.

The Q-band EPR spectrum of A_1^- in a nondeuterated PS I complex is compared with a spectral simulation of A_1^- in Figure 5B. The simulation was performed using the *g*-tensor extracted from the deuterated A_1^- spectrum in Figure 5A and an *A*-tensor of 9.0, 12.9 and 9.0 MHz.[44] Although it is less important for simulating a powder spectrum than for crystal studies, we used an axially symmetric hyperfine tensor transformed into the principal axis of gA_1. The simulation, which assumes that the A_{parallel} principal axis is collinear with the C(2)−CH_3 bond axis, accurately reproduces the major features of the Q-band spectrum of A_1^-, including the hyperfine couplings from the 3-methyl group. On the basis of the spectral simulations shown in Figure

TABLE 1: Number of Spins Attributed to A_1 and A_0 as a Function of Photoaccumulation Temperature in Perdeuterated PS I Complexes Isolated with DM from *Synechococcus* sp. PCC 7002

temperature	time	total spins/P700	A_1^-/P700$^+$	A_0^-/P700$^+$
205 K	1.5 h	1.05	1.0	0.05
212 K	0.5 h	1.4	0.97	0.43
220 K	0.5 h	1.3	0.97	0.33
240 K	0.6 h	~0	~0	~0

5A and B, the line width of A_1^- in the deuterated PS I complex is 2.2-fold narrower than in the nondeuterated PS I complex. When the simulated spectrum of A_1^- is subtracted from the experimental spectrum in Figure 5B, a derivative-shaped spectrum is extracted with a *g*-value of 2.0034 and a line width of 14 G which is characteristic of A_0^- (data not shown). Integration of the experimental spectra of the PS I complexes prepared with DM showed that the spectrum of A_1^- was contaminated with A_0^- at the relative spin concentration of 0.90:0.10. Although the effect is reproducible, the reason for the higher content of contaminating A_0^- in the nondeuterated compared to the perdeuterated PS I complexes under identical photoaccumulation conditions is not understood.

Absolute spin quantitations were first performed on A_1^- in the perdeuterated PS I complexes, for which the spectra of A_1^- and A_0^- are simplified and better resolved due to suppression of the hyperfine interactions. Table 1 shows the total number of spins of A_1^- per P700$^+$ in perdeuterated PS I complexes which were photoaccumulated at several temperatures. To determine the relative amounts of A_1^- and A_0^-, the A_1^- spectrum was simulated using the *g*-tensor determined from Figure 5A, scaled to the experimental spectrum by visually matching the g_{xx} and g_{yy}, components and its contribution subtracted from the experimental spectrum. At all temperatures below 240 K, the ratio of A_1^- reduced per P700 is $\leq$1.0. Illumination for longer times resulted in the generation of additional spins from a radical with a *g*-value of 2.0034 characteristic of A_0^-, with no additional increase in the number of spins derived from A_1^-. When the photoaccumulation was carried out in nondeuterated wild-type PS I complexes, the total number of spins per P700 as a function of temperature was found to be 0.4 at 240 K, 1.7 at 220 K, 1.5 at 215 K, 0.7 at 205 K, and 0.5 at 195 K. As the temperature is lowered from 215 to 205 K, the photoaccumulated spectrum changes from one with a relatively large contribution of A_0^- (similar in appearance to Figure 8, wild-type) to one with a relatively small contribution of A_0^- (similar in appearance to Figure 4B, solid line). Spectral simulations confirmed that the maximum number of spins from A_1^- was $\leq$1.0; any additional spins were derived from A_0^- (not shown).

Photoaccumulation of A_0^- and A_1^- in Wild-Type and Mutant PS I Complexes. PS I complexes lacking specific polypeptides can be categorized into two groups according to the location of the missing polypeptides relative to the C_3 axis of symmetry.[27] Group I includes the PS I complexes that are missing subunits on the side of the monomers where the (primed) m' and n' α-helices intersect, that is, proximal to the C_3 axis of symmetry. Thus, group I includes the complexes lacking the PsaI, PsaK, PsaL or PsaM polypeptides (see Figure 1A). Group II includes the PS I complexes that are missing subunits on the side of the monomers near the intersection of the (nonprimed) *m* and *n* α-helices. This group includes PS I complexes lacking the PsaE, PsaF, or PsaJ polypeptides (see Figure 1A). Regardless of whether group I (Figure 6) or group II (Figure 7) polypeptides are removed, the spectra of PS I complexes isolated with DM are similar to the wild-type PS I complexes for which A_1^- is the major photoaccumulated radical.

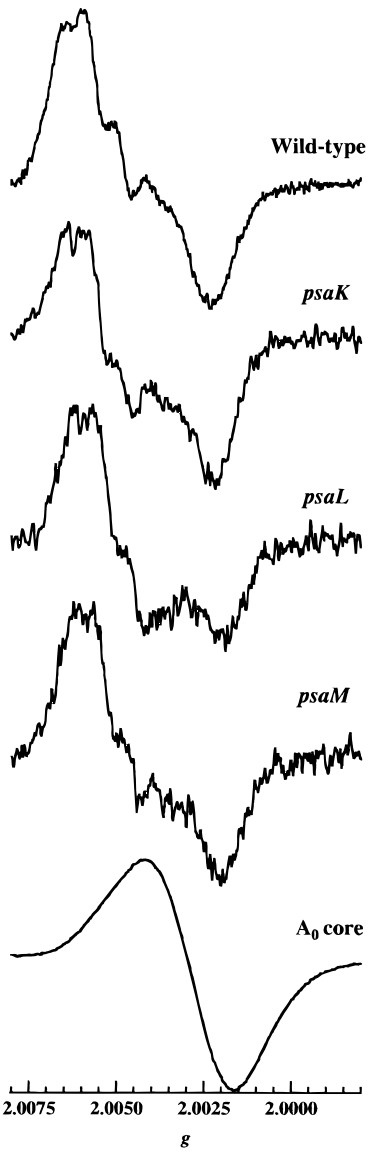

Figure 6. Q-band EPR spectra of PS I complexes from group I mutant strains isolated from *Synechococcus* sp. PCC 7002 with DM. The spectra of wild-type A_1^- (from Figure 4A, solid line), and A_0^- (from Figure 4B, dotted line) are shown at the top and bottom of the figure for comparison. The photoaccumulation was carried out for 40 min at 205 K. Instrument conditions: microwave power, 63 μW; modulation amplitude, 0.1 mT; modulation frequency, 100 kHz; temperature, 100 K; magnetic field scan, 1.2100 to 1.2200 T; microwave frequency, ca. 34.087 GHz. The wild-type and P700-A_0 core samples were signal-averaged 10 times; the mutant samples were signal-averaged 4 times.

Dramatically different results are obtained with some but not all of the PS I complexes prepared with TX-100. First, the Q-band EPR spectrum of a photoaccumulated PS I complex isolated with TX-100 contains a greater contribution from A_0^- (Figure 8, wild-type). Spectral simulations using an isotropic *g*-tensor for A_0^- and the *g*- and *A*-tensors for A_1^- in Figure 5B (dotted line) indicate that the spectrum of A_1^- in the nondeuterated PS I complex isolated with TX-100 is contaminated with A_0^- at a relative spin concentration of 0.65:0.35 (see Table 2). Second, removal of Group I polypeptides, either individually, or in combination with PsaL, leads to insignificant changes in the appearance of the photoaccumulated spectrum when compared with the wild-type (Figure 8). As shown in Table 2, the relative spin concentration of A_1^- to A_0^- after photoaccumu-

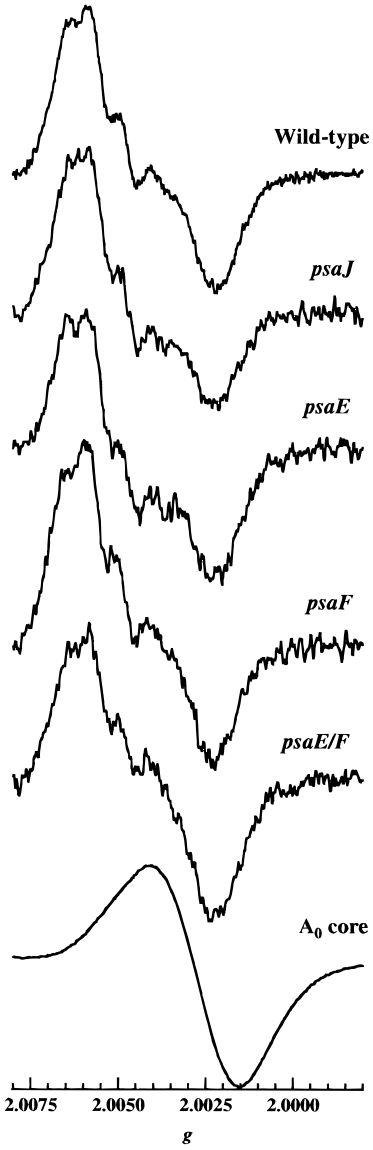

Figure 7. Q-band EPR spectra of PS I complexes from group II mutant strains isolated from *Synechococcus* sp. PCC 7002 with DM. The spectra of wild-type A_1^- (from Figure 4A, solid line), and A_0^- (from Figure 4B, dotted line) are shown at the top and bottom of the figure for comparison. The photoaccumulation was carried out for 40 min at 205 K. Experimental conditions are the same as those in Figure 6.

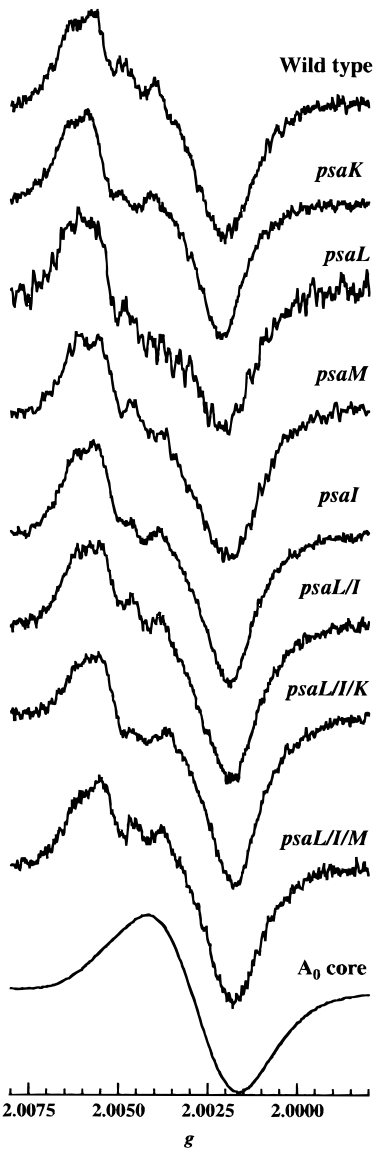

Figure 8. Q-band EPR spectra of PS I complexes from Group I mutant strains isolated from *Synechococcus* sp. PCC 7002 with TX-100. The spectra of wild-type A_1^- and A_0^- (from Figure 4B, dotted line) are shown at the top and bottom of the figure for comparison. The photoaccumulation was carried out for 40 min at 205 K. Experimental conditions are the same as those in Figure 6.

lation was invariant for PS I complexes lacking various group I polypeptides. However, when the group II polypeptide PsaF is removed, the high-field trough, which is derived primarily from a symmetrical radical with a *g*-value of 2.0034, has a significantly higher spin concentration relative to the $g = 2.0062$ component (Figure 9), which can still be identified as A_1^- by the presence of the hyperfine couplings. Spectral simulations show that in the PsaF mutant, the relative spin concentration of A_1^- to A_0^- is 0.45:0.55 (Table 2). When PsaE and PsaF are both removed, the resulting spectrum is derivative-shaped with a *g*-value of 2.0034 and a line width of 15 G and consists almost exclusively of A_0^- (Table 2). As noted above, the PS I complexes from the *psaF* and *psaE psaF* mutants are also depleted of PsaJ due to destabilization of PsaJ binding to the complex in the presence of TX-100, to polarity effects of the interposon fragment on the downstream *psaJ* gene, or for both reasons. However, as shown in Figure 9, the removal of PsaJ alone does not lead to the photoaccumulation of A_0^-, indicating that the increased appearance of A_0^- is predominantly a consequence of the removal of PsaF.

Effect of Reductant on the Wild-Type and *psaE psaF* Mutant PS I Complexes. To determine whether the appearance of photoaccumulated A_0^- in the *psaE psaF* mutant is a consequence of the dark chemical reduction of PhQ by sodium hydrosulfite, flash-induced optical absorption experiments were performed. The kinetics of the charge recombination between the electron acceptors and $P700^+$ of the *psaE psaF* mutant PS I complexes prepared with TX-100 and DM, measured in the presence of sodium ascorbate and DCPIP, were almost identical to wild-type PS I complexes prepared with TX-100 and DM (not shown). $P700^+$ reduction occurred on the tens-of milliseconds time scale due to the back-reaction from $[F_A/F_B]^-$, along with a slower reduction from the exogenous electron donor (DCPIP) on the seconds time scale (for assignments of the kinetics of $P700^+$ reduction see ref 60). The initial amplitudes of the absorbance change, as determined by a multiexponential fit, were very similar in the wild type and *psaE psaF* mutant

TABLE 2: Ratio of Photoaccumulated A_1^- to A_0^- in PS I Complexes Isolated from Wild-Type and Selected Mutant Strains of *Synechococcus* sp. PCC 7002

strain	detergent	A_1^-/A_0^- [a]
wild-type	DM	0.90:0.10
wild-type	TX-100	0.65:0.35
	Group I Polypeptides	
psaK	DM	0.85:0.15
psaK	TX-100	0.65:0.35
psaL	DM	0.95:0.05
psaL	TX-100	0.65:0.35
psaM	DM	0.90:0.10
psaM	TX-100	0.60:0.40
psaI	TX-100	0.65:0.35
psaI/L	TX-100	0.65:0.35
psaI/L/K	TX-100	0.65:0.35
psaI/L/M	TX-100	0.65:0.35
	Group II Polypeptides	
psaJ	DM	0.95:0.05
psaJ	TX-100	0.60:0.40
psaE	DM	0.85:0.15
psaE	TX-100	0.70:0.30
psaF	DM	0.90:0.10
psaF	TX-100	0.45:0.55
psaE/F	DM	0.80:0.20
psaE/F	TX-100	0.00:1.00

[a] The precision of the measurement is judged to be ca. 1 in 20.

PS I complexes. Equally important, there was virtually no difference between the wild-type and mutant PS I complexes under strongly reducing conditions. In the mutant PS I complex prepared with DM (Figure 10A) and TX-100 (Figure 10B), the major contribution to $P700^+$ reduction is brought about by two components with lifetimes of ca. 230 and 820 μs; these lifetimes are very close to those seen in the wild-type PS I complexes isolated from *Synechococcus* sp. PCC 7002 (not shown), and they are also in a good agreement with the lifetimes reported earlier for DM-PS I complexes isolated from *Synechocystis* sp. PCC 6803.[60] The faster, tens-of-microseconds component is attributed to the decay of ^{3}Chl in the core antenna, although some contribution from the A_1^- back-reaction cannot be excluded. Extrapolation of the multiexponential fit curve, upon exclusion of the latter fast component to the time-zero yields initial amplitudes of the absorbance change (Figure 10B) that are reasonably close to those seen in the presence of DCPIP (not shown). These results show that chemical reduction of the terminal iron−sulfur clusters F_A and F_B is not accompanied by reduction of any of the earlier electron carriers. Therefore, the dark chemical reduction of A_1 in the PS I complex isolated with TX-100 from the *psaE psaF* mutant can be ruled out, and the occurrence of the A_0^- radical can be attributed to prolonged illumination at 205 K.

Steady-State Rates of Flavodoxin Reduction. Steady-state rates of flavodoxin photoreduction were measured in wild-type and mutant PS I complexes to determine whether the occurrence of the photoaccumulated A_0^- radical correlates with a loss of throughput of electrons from the physiological donor, cytochrome c_6. As depicted in Table 3, wild-type PS I complexes prepared with DM gave the highest rates of flavodoxin photoreduction, which correspond to a throughput of ca. 120 electrons transferred per reaction center per second. PS I complexes prepared with TX-100 generally had slightly lower rates of flavodoxin reduction for a given mutant strain. Except for a slight decrease in the rate of flavodoxin reduction in the *psaK* and *psaM* mutants, the removal of group I polypeptides had little effect. The removal of group II polypeptides results in a lower rate of flavodoxin reduction, and in particular, PS I

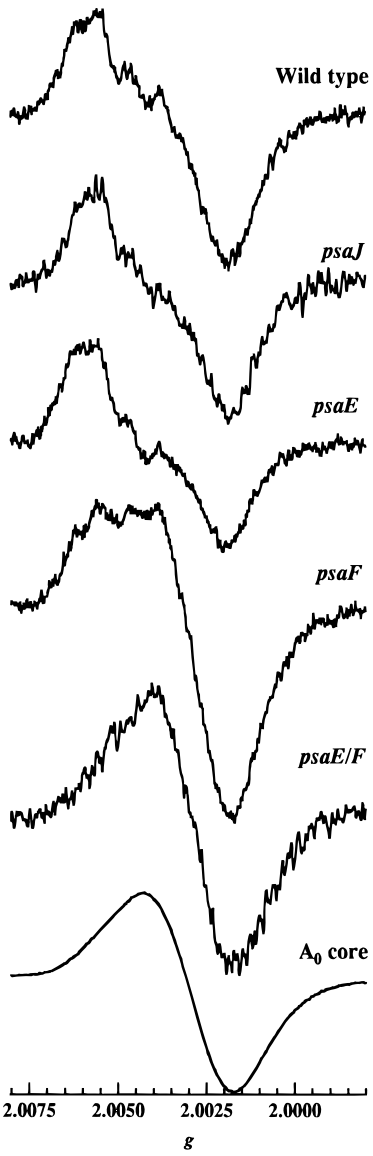

Figure 9. Q-band EPR spectra of PS I complexes from group II mutant strains isolated from *Synechococcus* sp. PCC 7002 with TX-100. The spectra of wild-type A_1^- and A_0^- (from Figure 4B, dotted line) are shown at the top and bottom of the figure for comparison. The photoaccumulation was carried out for 40 min at 205 K. Experimental conditions are the same as those in Figure 6.

complexes lacking PsaE and PsaF showed the lowest rates; nevertheless, the rates were identical for the PS I complexes prepared with DM and the TX-100. In both instances, the rates of electron throughput were about 2-fold lower than for the wild-type PS I complexes. Some of this effect might be due to altered interactions of flavodoxin with PsaC that could occur when PsaE is missing from the acceptor side.[34,35] Regardless of the detergent used and despite the loss of peripheral polypeptides, the mutant PS I complexes studied here retain a reasonably high capacity for steady-state electron transport to flavodoxin. Hence, the presence of the loss of the ability to observe the photoaccumulated A_1^- radical in the *psaE psaF* mutant PS I complex prepared with TX-100 does not correlate with an inability to reduce flavodoxin under conditions of steady-state illumination.

Phylloquinone Content of PS I. One further explanation for the appearance of the photoaccumulated A_0^- radical in the *psaE psaF* mutant prepared with Triton X-100 is that phylloquinone is lost from the A_1 binding site. Only the PS I complex

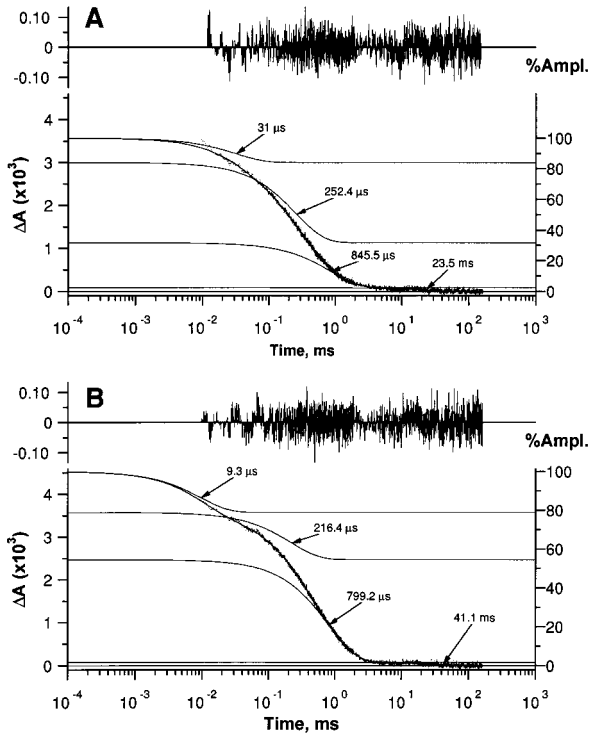

Figure 10. Kinetics of flash-induced absorbance changes (ΔA) at 832 nm of *psaE psaF* mutant PS I complexes in 0.02% DM (A) and 0.02% TX-100 (B). The PS I complexes were suspended in 100 mM glycine buffer, pH 10, and 100 mM sodium hydrosulfite at a chlorophyll concentration of 50 μg mL^{-1}. The plots depict an average of 16 traces acquired at 5 s intervals. Results of the multiexponential fit are displayed as the fit curve, individual exponential components, and residuals of the fit. Each individual component is plotted with vertical offset relative to the next component (with a longer lifetime) or the base line, the offset being equal to the amplitude of the latter component.

from the *psaE psaF* mutant prepared with TX-100 was selected for analysis because the EPR spectrum showed the lowest content of photoaccumulated A_1^- and because the rate of flavodoxin reduction catalyzed was the lowest of all the PS I mutants tested. The phylloquinone content of the wild-type PS I complex was 2.5 per 100 Chl, while the phylloquinone content of the *psaE psaF* mutant was 2.6 per 100 Chl. Both the steady-state flavodoxin reduction rate data and chemical analyses therefore indicate that the failure to photoaccumulate the A_1^- radical in the *psaE psaF* mutant is not due to the loss of the redox-active phylloquinone from its binding site.

Discussion

Phylloquinone is reduced to phyllohydroquinone in two one-electron steps which are described by the redox potentials $E_{1/2}(Q/Q^{-\bullet})$ for the phylloquinone-phyllosemiquinone couple and $E_{1/2}(Q^{-\bullet}/Q^{2-})$ for the phyllosemiquinone−phyllohydroquinone couple. These two single-electron steps are related to the two-electron phylloquinone−phyllohydroquinone couple by the following equation:

$$E_{1/2}(Q/Q^{2-}) = {}^1/_2(E_{1/2}(Q/Q^{-\bullet}) + E_{1/2}(Q^{-\bullet}/Q^{2-}))$$

The $E_{1/2}(Q/Q^{-\bullet})$ value in aqueous solution at neutral pH containing 5 M 2-propanol and 2 M acetone has been measured to be −170 mV vs NHE.[15] The $E_{1/2}(Q/Q^{-\bullet})$ value is further defined by dependence on the solution pH according to the following equation:

TABLE 3: Rates of Flavodoxin Reduction for PS I Complexes Isolated from Wild-Type and Selected Mutant Strains of *Synechococcus* sp. PCC 7002[a]

strain	detergent	rate[b]	e^- RC^{-1} s^{-1} [c]	% wild type[d]
wild-type	DM	4710 ± 180	118 ± 4.5	100
wild-type	TX-100	4620 ± 320	114 ± 8.0	97
		Group I Polypeptides		
psaK	DM	3320 ± 250	83 ± 6.3	70
psaK	TX-100	3000 ± 230	75 ± 5.8	64
psaL	DM	4255 ± 131	106 ± 3.2	89
psaL	TX-100	4062 ± 102	102 ± 2.6	86
psaM	DM	3527 ± 139	88 ± 3.5	75
psaM	TX-100	3436 ± 120	86 ± 3.0	72
psaI	TX-100	4115 ± 172	103 ± 4.3	87
psaI/L	TX-100	4449 ± 507	111 ± 12.7	94
psaI/L/K	TX-100	4258 ± 370	106 ± 9.3	89
psaI/L/M	TX-100	4122 ± 490	103 ± 12.2	87
		Group II Polypeptides		
psaJ	DM	3530 ± 100	88 ± 2.5	75
psaJ	TX-100	3270 ± 110	82 ± 2.8	69
psaE	DM	3390 ± 340	83 ± 9.3	70
psaE	TX-100	3330 ± 370	81 ± 8.5	69
psaF	DM	2900 ± 170	73 ± 4.3	62
psaF	TX-100	2420 ± 140	61 ± 3.5	52
psaE/F	DM	2410 ± 100	60 ± 1.5	51
psaE/F	TX-100	2150 ± 150	54 ± 3.8	46

[a] Each measurement is the average of four individual measurements. [b] Rate expressed as micromoles flavodoxin reduced h^{-1} mg Chl^{-1}. [c] Rate expressed as number of electrons transferred per second per 100 Chl (equivalent to electrons transferred per second per reaction center at 100 Chl/P700). [d] Percentage of rate for wild-type PS I complex prepared with DM.

$$E_{1/2}(Q/Q^{-\bullet}) = E_7(Q/Q^{-\bullet}) + 59\ \log((k_i + [H+])/k_i + 10^{-7}))$$

where k_i is the ionization constant.[15] The pK_a of the Vitamin K_1 semiquinone is 5.5[42] (although this value is considered too high due to the high percentage of alcohol necessary to dissolve this hydrophobic molecule.[54]) The pK_a of the Vitamin K_1 semiquinone in water is estimated to be about 4.5, a value similar to the measured pK_a of 4.3 for the more soluble 2,3-dimethyl-1,4-naphthoquinone.[54] At neutral pH in aqueous solution, the singly reduced phyllosemiquinone anion radical is therefore unprotonated. The value of $E_{1/2}(Q^{-\bullet}/Q^{2-})$ in aqueous solution at neutral pH containing 5 M 2-propanol and 2 M acetone is +220 mV vs NHE, a value 390 mV more electropositive than the first step of reduction.[15] Although we are unaware of a comprehensive pH-$E_{1/2}$ diagram for phylloquinone, the pH−$E_{1/2}$ diagram for the *p*-benzoquinone/hydroquinone couples shows that in the region above the pK_a for hydroquinone, i.e., pH 12, the $E_{1/2}$ for the single-electron reduction of benzosemiquinone to unprotonated hydroquinone is more electronegative than for the single-electron reduction of benzoquinone to benzosemiquinone.[11] However, if the second single-electron reduction is carried out at pH values below 10 where protonation can occur, the $E_{1/2}$ for the single electron reduction of benzosemiquinone to protonated hydroquinone is considerably more electropositive than the single-electron reduction of benzoquinone to benzosemiquinone (the $E_{1/2}$ is pH-dependent between 4 and 10).[1] This corresponds to the trend noted above for the $E_{1/2}$ values of single and double reduction steps of phylloquinone on aqueous solution.

The properties of the redox-active A_1 phylloquinone in PS I are markedly different than those of phylloquinone in aqueous solution. The midpoint potential of A_1 in PS I has not been measured directly, but a value of −810 mV is derived from calculations based on the kinetics of electric field-induced electron-transfer rates,[61] and a similar value of −800 mV is

derived from calculations based on the P700 triplet yield.[50] The single electron transfer from A_0 to A_1 results in the formation of a phyllosemiquinone anion radical.[19,32,55] The quinone-binding domain is considered to be hydrophobic with a size similar to that of anthraquinone and with a H-bond or a $\pi-\pi$ electronic interaction between the quinone and the binding site.[24] Alternately, the larger anisotropy of cyanobacterial A_1^- compared with reduced Vitamin K_1^- may result from H-bonds to protein or Coulombic interactions with charged amino acid residues in the binding pocket.[57] Therefore the environment of the A_1 binding site and not the inherent properties of phylloquinone confer the highly negative reduction potential to this electron acceptor.

The premise throughout this work is that A_0^- is generated during photoaccumulation treatment of PS I samples when A_1 becomes unable to carry out electron transfer.[49] Two conditions meet this criterion: physical removal of the redox-active phylloquinone from its binding site[62] and reduction of A_1 to the doubly reduced state.[7] In the singly reduced state, A_1^- is paramagnetic and becomes EPR-visible. In the doubly reduced state, A_1^{2-} is diamagnetic and becomes EPR-silent. Whether single or double reduction of A_1 occurs depends on the reduction state of the electron acceptors and on the environment of the binding site. In wild-type PS I complexes photoaccumulation at room temperature in the presence of sodium hydrosulfite[49] or redox poising at ca. -600 mV in the presence of methyl viologen in darkness results in 1) the inhibition of electron transfer from A_0 to A_1 and in the appearance of fast recombination kinetics between $P700^+$ and A_0^- [7] and 2) the disappearance of the electron spin-polarized EPR spectrum assigned to the radical pair composed of oxidized P700 and reduced phylloquinone.[52] These effects are interpreted as a consequence of the double reduction of A_1. In the *psaF* and *psaE psaF* mutant, photoaccumulation at 205 K in the presence of sodium hydrosulfite results in the loss of the A_1^- EPR signal and the appearance of the A_0^- EPR signal. This is consistent with the double reduction of A_1 to the diamagnetic state.

We suggest that in the hydrophobic binding pocket, a second electron reduction of A_1^- in PS I is energetically prohibitive when it is not accompanied by a protonation step. To our knowledge, no pH vs $E_{1/2}$ data are available for Vitamin K_1, making it difficult to estimate this reduction potential. However, the effect of pH on the second electron reduction step of hydroquinone has been measured. The $E_{1/2}(Q^{-\bullet}/Q^{2-})$ is $+459$ mV at pH 7.0 and $+23$ mV at pH 13.5, a difference of 435 mV. If we assume that the phylloquinone binding pocket is similarly aprotic, then we might expect that the reduction potential would be driven highly negative and could exceed that of the first electron reduction step. This may be the primary reason that the double reduction of A_1 is a rare event in PS I. That flavodoxin reduction occurs at a rate ca. 50% of the wild-type indicates that the majority of A_1 continues to function normally between the oxidized and semiquinone states at room temperature. Even if a water channel were opened in the vicinity of the quinone, the first reduction step may not result in protonation due to the low pK_a of phyllosemiquinone anion radical. However, if protonation could occur concomitant with the second reduction step, then the energetics of the second electron reduction would be considerably more favorable. This assessment of the energetics of the single- and double-electron reduction complies with the experimental finding that the midpoint potential of the semiphylloquinone/phylloquinol couple is higher than that of the phylloquinone/semiphylloquinone couple in isolated PS I complexes.[7] This also agrees with what occurs with Q_B in PS II, for which the second electron reduction of plastosemiquinone occurs concomitant with protonation to form plastohydroquinone.[40] Indeed, in the purple bacterial reaction center the double reduction of Q_A is known to occur[39] and in PS II the double reduction of Q_A is accompanied by protonation to Q_AH_2.[25,58,59] Our working hypothesis is that the removal of the PsaF polypeptide and particularly the simultaneous removal of the PsaF and PsaE polypeptides in PS I opens a water channel to the redox-active phylloquinone so that the second reduction step can be accompanied by protonation of phyllosemiquinone to phyllohydroquinone. The analytical results showing the retention of two phylloquinones per P700 supports the proposal that double reduction of A_1 to the EPR-silent, diamagnetic state has occurred. The inability of A_1 to function as an electron donor or acceptor then leads to the photoaccumulation of the A_0^- radical.

A corollary of this hypothesis is that if only one of the two branches active in electron transfer, then only the removal of peripheral proteins on the side of the PS I complex containing the redox-active phylloquinone should alter the environment and photoaccumulation behavior for A_1^-. Removal of peripheral proteins on the side of the PS I complex containing the nonredox active phylloquinone should have no effect on the EPR properties of A_1^-. If, however, both branches were active in electron transfer, removal of peripheral proteins on either side of the PS I complex would lead to a changed environment for only one-half of the population of A_1^-. Removal of proteins on both sides of the PS I complex would then be necessary for A_1^- to become EPR-silent. One argument against the presence of two redox-active phylloquinones is that a maximum of 1.0 spins of A_1^- can be accumulated per spin of $P700^+$ at a variety of photoaccumulation temperatures (Table 1). Spins in excess of 1.0 A_1^- per $P700^+$ are invariably derived from the A_0^- radical. The use of Q-band EPR spectroscopy has allowed for the first time the ratio of spins in A_0^- to A_1^- in an admixture to be determined by simulation protocols, which serves as a crucial cross-check on the absolute spin quantitation of the two radicals (see Table 2). A second argument against the presence of two redox-active A_1 species is that only the removal of the PsaF or PsaE and PsaF polypeptide(s) at the C_3-distal edge of the PS I complex results in the disappearance of A_1^- and the appearance of A_0^-. The removal of C_3-proximal polypeptides PsaK, PsaI, PsaL, or PsaM either singly or in combination near the C_3 symmetry axis or at the interfaces between trimers had no effect on the photoaccumulation of A_1^-.

The double reduction of A_1 is an unlikely event, even in the *psaE psaF* mutant, but it can be promoted by the appropriate choice of detergent, photoaccumulation times, and photoaccumulation temperatures. The increased amounts of A_0^- observed in wild-type PS I complexes after low-temperature photoaccumulation of PS I complexes isolated with TX-100 may reflect the extraction of limited amounts of PsaF and/or PsaE as illustrated in Figure 3. Thus, one conclusion from these studies is that the use of Triton X-100 should be avoided in the preparation of native PS I complexes because of the difficulty in controlling the extraction of PsaE and PsaF as well as perturbation of the properties of A_1. Although the specific effect of TX-100 in modification of the A_1 binding site is not known, some possibilities can be suggested. PsaF appears to bind two to four chlorophyll molecules, and the loss of this polypeptide could create a more hydrophilic environment in this region of the PS I complex. The absence of PsaF could additionally render chlorophylls bound to the cyanobacterial reaction center susceptible to removal by TX-100, which could further modify

the environment of A_1. In the absence of both PsaF and PsaE, TX-100 may further modify the polypeptide environment around A_1 by changing the packing of the α-helices in this region of the PS I complex. Any or all of these scenarios could result in the opening of a water channel that may facilitate the protonation of the phyllosemiquinone anion radical. In support of these suggestions, the absorption spectra of PS I complexes isolated with TX-100 are blue-shifted and broadened relative to those of complexes prepared with DM (G. Shen and I. Vassiliev, unpublished results).

Several previous studies have noted differences in the appearance of photoaccumulated EPR spectra depending on the detergent used to isolate PS I particles. The photoaccumulated, X-band EPR spectrum of PS I complexes prepared from higher plants (spinach) using digitonin, a relatively mild detergent, shows an asymmetry[20] which is now known to be due to the presence of unresolved hyperfine couplings on A_1^-. In contrast, the spectrum of the identical PS I complexes prepared using TX-100 has lost much of the hyperfine structure so that it is not as broad as that found for the digitonin preparations and therefore not as easily distinguished from A_0^-.[21] These differences were attributed to a perturbation of the structure of the PS I complex induced by TX-100.[32] On the basis of the ability of TX-100 to remove PsaF (then known as subunit III) from Swiss Chard PS I complexes[3] and on the propensity of TX-100 to extract up to 60 chlorophylls from barley[36] and spinach[18] PS I complexes, the perturbation may well represent the loss of both PsaF (and possibly other low molecular mass polypeptides) and chlorophylls from the higher plant PS I complexes. By analogy with findings in this study on the cyanobacterial PS I complex, we propose that the loss of PsaF and chlorophyll in the higher plant PS I complexes leads to facile double reduction of A_1 and the subsequent appearance of the $g = 2.0037$ resonance attributed to A_0^-. Our results, however, differ from those of Mansfield[32] in the spin quantitation of A_1^-. We find that the maximum number of spins that can be attributed to A_1^- in cyanobacterial PS I complexes prepared with DM is 1.0 (this work), whereas the maximum number of spins that can be attributed to A_1^- in higher plant digitonin PS I particles is 2.0.[32] Although the number of spins that can be accumulated in A_1 may be species specific or depend on extremely subtle factors in the photoaccumulation protocol, our results do not support the reduction of the second phylloquinone in PS I under the photoaccumulation conditions described in this study.

In the most recent model for PS I,[48] a well-defined area of electron density directly adjacent to the short connection between α-helices *m*′ and *n*′ was observed and tentatively assigned as phylloquinone Q_K. This region is nearly perfectly conserved in amino acid sequence between PsaA and PsaB and is partially conserved in the PshA and PscA reaction center polypeptides as deduced from the DNA sequence of heliobacteria[29] and green sulfur bacteria,[9] respectively. This electron density lies in close proximity to the other components of the electron transport chain and lies between the eC_3 chlorophyll and the F_X cluster. Moreover, the distance (25 Å ± 1 Å) and angle (26° ± 2°) of this electron density relative to P700 are in close agreement with the experimentally determined values of 25.4 Å ± 0.3 Å and 26° ± 0.5°.[4,66] It is presumed that a second phylloquinone would be bound near the short connection between α-helices *m* and *n*, although the electron density that could be assigned to the Q_K′ quinone observed in this symmetry-related position appears to be occupied by a tilted *m*′ transmembrane helix (Figure 1B). However, given that there are two phylloquinone molecules per PS I complex, it is possible that this ambiguity will be removed when the crystal structure is available at higher resolution.

The model for PS I based on the 4 Å data set depicts *m* and *m*′ as transmembrane helices and *n* and *n*′ as stromal surface helices (Figure 1A). The *n* helix extends over a region occupied by membrane-spanning primed helices, and the *n*′ helix extends over a region occupied by membrane-spanning nonprimed helices. The intersection of the *m* and *n* helices contains a group of conserved aromatic residues which have some similarity to a portion the Q_B binding site of bacterial reaction centers. The *n* helix is equivalent to the 12-residue helix in the bacterial reaction center which connects transmembrane helices D and E, and which also forms a portion in the Q_B binding site of the L subunit of the bacterial reaction center. The binding site contains a number of amino acid residues that have been implicated in protonation of Q_B.[38] In the region most distal from the C_3 symmetry axis of the trimer, the *n* helix abuts the region occupied by the membrane spanning PsaF/PsaJ polypeptides, whereas the region of the *n*′ helix most distant from the pseudo-2-fold axis C_2 (AB) abuts the region occupied by the membrane-spanning PsaL/PsaI and (to a lesser degree) PsaK polypeptides. Since the removal of PsaF (and to an even greater degree both PsaE and PsaF) results in the photoaccumulation of A_0^-, we conclude that the quinone which is active in electron transport is bound near the intersection of the nonprimed *m* and *n* helices.

Conclusions

Electron transfer in the *Rhodobacter sphaeroides* reaction center is known to occur only through the BPh(L) branch of electron carriers (reviewed in Kirmayer[26]). Few, if any, studies have addressed the question of whether electron transfer in PS I occurs through one or both branches of the pseudo-symmetric pairs of chlorophylls. Based on the finding that the A_1^- radical was replaced with the A_0^- radical in the *psaE psaF* mutant, we propose that electron transfer is unidirectional through that phylloquinone which is located on the nonprimed *m* and *n* helices in PS I. By analogy to the pathway of electron transport in bacterial reaction centers, we suggest that the active pathway for electron transport is as follows: $eC_1 \rightarrow eC_2' \rightarrow eC_3' \rightarrow Q_K \rightarrow F_X$. As a final comment, it is also worth noting that even in homodimeric iron−sulfur type reaction centers represented by green sulfur bacteria[10] and heliobacteria,[29] electron transport could occur unidirectionally because of asymmetry introduced by interactions with low-molecular-mass polypeptides.

Acknowledgment. The authors thank A. Kamlowski, D. Stehlik, and A. Van der Est for advice on the simulation of A_1 and F. MacMillan, R. Bittl and S. Zech for discussions on the spectroscopic properties of A_1. This work was supported by National Science Foundation Grants MCB-9723661 (to J.H.G.) and MCB-9723469 (to D.A.B).

References and Notes

(1) Bailey, S. I.; Ritchie, I. M.; Hewgill, F. R. *J. Chem. Soc., Perkin Trans.* **1983**, *2*, 645.
(2) Barry, B. A.; Bender, C. J.; McIntosh, L.; Ferguson-Miller, S.; Babcock, G. T. *Isr. J. Chem.* **1988**, *28*, 129.
(3) Bengis, C.; Nelson, N. *J. Biol. Chem.* **1977**, *252*, 4564.
(4) Bittl, R.; Zech, S. G.; Fromme, P.; Witt, H. T.; Lubitz, W. *Biochemistry* **1997**, *36*, 12001.
(5) Blum, H.; Beier, H.; Gross, H. J. *Electrophoresis* **1987**, *8*, 93.
(6) Bonnerjea, J.; Evans, M. C. W. *FEBS Lett.* **1982**, *148*, 313.
(7) Bottin, H.; Sétif, P. *Biochim. Biophys. Acta* **1991**, *1057*, 331.
(8) Brettel, K. *Biochim. Biophys. Acta* **1997**, *1318*, 322.

(9) Büttner, M.; Xie, D.; Nelson, H.; Pinther, W.; Hauska, G.; Nelson, N. *Proc. Natl. Acad. Sci. U.S.A.* **1992**, *89*, 8135.
(10) Büttner, M.; Xie, D.; Nelson, H.; Pinther, W.; Hauska, G.; Nelson, N. *Biochim. Biophys. Acta* **1992**, *1101*, 154.
(11) Chambers, J. Q. In *The Chemistry of the Quinonoid Compounds*; Patai, S., Rappoport, Z., Eds.; John Wiley and Sons: New York, 1988; Vol. II., p 719.
(12) Chitnis, V. P.; Chitnis, P. R. *FEBS Lett.* **1993**, *336*, 330.
(13) Dawson, R. M. C.; Elliott, D. C.; Elliott, W. H.; Jones, K. M. *Data for Biochemical Research*, 3rd ed.; Clarendon Press: Oxford, 1986.
(14) Deisenhofer, J.; Epp, O.; Miki, K.; Huber, R.; Michel, H. *Nature* **1985**, *318*, 618.
(15) Depew, M. C.; Wan, J. K. S. In *The Chemistry of the Quinonoid Compounds*; Patai, S., Rappoport, Z., Eds.; John Wiley and Sons: New York, 1988; Vol. II, p 963.
(16) Ermler, U.; Michel, H.; Schiffer, M. *J. Bioenerg. Biomembr.* **1994**, *26*, 5.
(17) Golbeck, J.; Bryant, D. In *Current Topics in Bioenergetics*; Lee, C. P., Ed.; Academic Press: San Diego, 1991; Vol. 16, p 83.
(18) Golbeck, J. H.; Lien, S.; San Pietro, A. *Arch. Biochem. Biophys.* **1977**, *178*, 140.
(19) Gulin, V. I.; Bouman, M. K.; Dikanov, S. A.; Tsvetkov, Y. D. *Dokl. Akad. Nauk SSSR* **1991**, *318*, 1246.
(20) Heathcote, P.; Evans, M. C. W. *FEBS Lett.* **1980**, *111*, 381.
(21) Heathcote, P.; Hanley, J. A.; Evans, M. C. W. *Biochim. Biophys. Acta* **1993**, *1144*, 54.
(22) Heathcote, P.; Moënne-Loccoz, P.; Rigby, S. E. J.; Evans, M. C. W. *Biochemistry* **1996**, *35*, 6644.
(23) Hecks, B.; Wulf, K.; Breton, J.; Leibl, W.; Trissl, H. W. *Biochemistry* **1994**, *33*, 8619.
(24) Iwaki, M.; Itoh, S. *Biochemistry* **1991**, *30*, 5347.
(25) Kirilovsky, D.; Rutherford, A. W.; Etienne, A. L. *Biochemistry* **1994**, *33*, 3087.
(26) Kirmayer, C.; Holten, D. *Photosyn. Res.* **1987**, *13*, 225.
(27) Krauss, N.; Schubert, W. D.; Klukas, O.; Fromme, P.; Witt, H. T.; Saenger, W. *Nature Struct. Biol.* **1996**, *3*, 965.
(28) Lichtenthaler, H. K. *Methods Enzymol.* **1987**, *148*, 350.
(29) Liebl, U.; Mockensturm-Wilson, M.; Trost, J. T.; Brune, D. C.; Blankenship, R. E.; Vermaas, W. *Proc. Natl. Acad. Sci. U.S.A.* **1993**, *90*, 7124.
(30) MacKinney, G. *J. Biol. Chem.* **1941**, *140*, 315.
(31) MacMillan, F.; Hanley, J.; van der Weerd, L.; Knupling, M.; Un, S.; Rutherford, A. W. *Biochemistry* **1997**, *36*, 9297.
(32) Mansfield, R. W.; Evans, M. C. W. *Isr. J. Chem.* **1988**, *28*, 97.
(33) McCracken, J. L.; Sauer, K. *Biochim. Biophys. Acta* **1983**, *724*, 83.
(34) Mühlenhoff, U.; Kruip, J.; Bryant, D. A.; Rögner, M.; Sétif, P.; Boekema, E. *EMBO J.* **1996**, *15*, 488.
(35) Mühlenhoff, U.; Zhao, J.; Bryant, D. A. *Eur. J. Biochem* **1996**, *235*, 324.
(36) Mullet, J. E.; Burke, J. J.; Arntzen, C. J. *Plant Physiol.* **1980**, *65*, 814.
(37) Norris, R. J.; Uphaus, R. A.; Crespi, H. L.; Katz, J. J. *Proc. Natl. Acad. Sci. USA* **1971**, *68*, 625.
(38) Okamura, M.; Feher, G. In *Anoxygenic Photosynthetic Bacteria*; Blankenship, R., Madigan, M. T., Bauer, C. E., Eds.; Kluwer: Dordrecht, 1995; p 577.
(39) Okamura, M.; Isaacson, R. A.; Feher, G. *Biochim. Biophys. Acta* **1979**, *546*, 394.
(40) Paddock, M. L.; McPherson, P. H.; Feher, G.; Okamura, M. Y. *Proc. Natl. Acad. Sci. U.S.A.* **1990**, *87*, 6803.
(41) Parrett, K. G.; Mehari, T.; Warren, P. G.; Golbeck, J. H. *Biochim. Biophys. Acta* **1989**, *973*, 324.
(42) Patel, K. B.; Willson, R. L. *J. Chem. Soc., Faraday Trans. 1* **1973**, *69*, 814.
(43) Prisner, T. F.; McDermott, A. E.; Un, S.; Norris, J. R.; Thurnauer, M. C.; Griffin, R. G. *Proc. Natl. Acad. Sci. U.S.A.* **1993**, *90*, 9485.
(44) Rigby, S. E. J.; Evans, M. C. W.; Heathcote, P. *Biochemistry* **1996**, *35*, 6651.
(45) Schägger, H.; von Jagow, G. *Anal. Biochem.* **1987**, *166*, 368.
(46) Schluchter, W.; Bryant, D. Ph.D. Thesis, The Pennsylvania State University, University Park, PA, 1995.
(47) Schluchter, W. M.; Shen, G. H.; Zhao, J. D.; Bryant, D. A. *Photochem. Photobiol.* **1996**, *64*, 53.
(48) Schubert, W. D.; Klukas, O.; Krauss, N.; Saenger, W.; Fromme, P.; Witt, H. T. *J. Mol. Biol.* **1997**, *272*, 741.
(49) Sétif, P.; Bottin, H. *Biochemistry* **1989**, *28*, 2689.
(50) Sétif, P.; Bottin, H.; Brettel, K. In *Current Research Photosynthesis, Proceedings of the International Conference Photosynthesis*; Baltscheffsky, M., Ed.; Kluwer: Dordrecht, Netherlands, 1990; Vol. 2, p 539.
(51) Shen, G.; Bryant, D. A. *Photosynth. Res.* **1995**, *44*, 41.
(52) Snyder, S. W.; Rustandi, R. R.; Biggins, J.; Norris, J. R.; Thurnauer, M. C. *Proc. Natl. Acad. Sci. U.S.A.* **1991**, *88*, 9895.
(53) Stevens, S. E., Jr.; Patterson, C. O. P.; Myers, J. *J. Phycol.* **1973**, *9*, 427.
(54) Swallow, A. J. In *Functions of Quinones in Energy Conserving Systems*; Academic Press: New York, 1982; p 59.
(55) Thurnauer, M. C.; Brown, J. W.; Gast, P.; Feezel, L. L. *Radiat. Phys. Chem.* **1989**, *34*, 647.
(56) Thurnauer, M. C.; Gast, P. *Photobiochem. Photobiophys.* **1985**, *9*, 29.
(57) van der Est, A.; Prisner, T.; Bittl, R.; Fromme, P.; Lubitz, W.; Möbius, K.; Stehlik, D. *J. Phys. Chem. B* **1997**, *101*, 1437.
(58) VanMieghem, F.; Brettel, K.; Hillmann, B.; Kamlowski, A.; Rutherford, A. W.; Schlodder, E. *Biochemistry* **1995**, *34*, 4798.
(59) Vass, I.; Styring, S.; Hundal, T.; Koivuniemi, A.; Aro, E.; Andersson, B. *Proc. Natl. Acad. Sci. U.S.A.* **1992**, *89*, 1408.
(60) Vassiliev, I. R.; Jung, Y. S.; Smart, L. B.; Schulz, R.; McIntosh, L.; Golbeck, J. H. *Biophys. J.* **1995**, *69*, 1544.
(61) Vos, M. H.; Van Gorkom, H. J. *Biochim. Biophys. Acta* **1988**, *934*, 293.
(62) Warren, P. V.; Golbeck, J. H.; Warden, J. T. *Biochemistry* **1993**, *32*, 849.
(63) Warren, P. V.; Parrett, K. G.; Warden, J. T.; Golbeck, J. H. *Biochemistry* **1990**, *29*, 6545.
(64) Witt, I.; Witt, H. T.; Gerken, S.; Saenger, W.; Dekker: J. P.; Rögner, M. *FEBS Lett.* **1987**, *221*, 260.
(65) Yang, F.; Shen, G.; Schluchter, W. M.; Zybailov, B.; Ganago, A.; Golbeck, J. H.; Bryant, D. In *The Photosynthetic Prokaryotes*; Peschek, G. A., Loeffelhardt, W., Schmetterer, G., Eds.; Plenum Press: New York, 1998. In press.
(66) Zech, S. G.; van der Est, A. J.; Bittl, R. *Biochemistry* **1997**, *36*, 9774.